Contribution from the Instituto de Desarrollo Tecnológico para la Industria Química, Güemes 3450, 3000 Santa Fe, Argentina, and Departamento de Física, Facultad de Ciencias Exactas, Universidad Nacional de La Plata, C.C.67, 1900 La Plata, Argentina

Molecular Structure of Bis(L-leucinato)zinc(II) and Single-Crystal EPR Spectra of the Substitutionally ^{63}Cu(II)-Doped Complex

C. A. Steren,*[†,1a] R. Calvo,[†,1b] O. E. Piro,[‡,1b] and B. E. Rivero[‡,1c]

Received September 15, 1988

The title compound, $Zn[H_2NCHCO_2CH_2CH(CH_3)_2]_2$ (abbreviated as Zn(L-Leu)$_2$), crystallizes in the monoclinic system, space group $P2_1$, with a = 9.584 (4) Å, b = 5.389 (2) Å, c = 14.866 (3) Å, β = 106.84 (3)°, and Z = 2. The structure was solved by X-ray diffraction techniques employing 1355 independent reflections and refined by the least-squares method to an agreement factor R = 0.048. The two L-leucine molecules per formula unit act as bidentate ligands of the Zn(II) ion, forming a N_2O_2 squashed tetrahedral configuration. The carboxyl oxygen of a third amino acid molecule completes a pentagonal coordination around Zn(II). The crystal structure of Zn(L-Leu)$_2$ was compared to the quasi-isomorphous structure of the Cu(L-Leu)$_2$ complex. Room-temperature EPR data of substitutional ^{63}Cu(II) impurities in single crystals of Zn(L-Leu)$_2$ were taken at 34 GHz. From these data we obtained g^1 = 2.273 (1), g^2 = 2.055 (1), g^3 = 2.066 (1), A^1_{Cu} = 167.3 (2) × 10^{-4} cm^{-1}, A^2_{Cu} = 0 (8) × 10^{-4} cm^{-1}, and A^3_{Cu} = 11 (2) × 10^{-4} cm^{-1} for the principal values of the gyromagnetic (**g**) and copper hyperfine ($\mathbf{A}_{Cu}$) tensors. The principal directions corresponding to g^1 and to A^1_{Cu} are nearly the same and reflect the orientation of the molecules in the crystal. The hyperfine coupling with the nuclei of the two ^{14}N ligands to copper is partially resolved for certain field orientations. In these orientations we observe differences on the order of 15% between the hyperfine interactions of the two nitrogens. By computer simulation of the spectra, we obtained A^1_N = 12 (1) × 10^{-4} cm^{-1}, A^2_N = 9 (1) × 10^{-4} cm^{-1}, and A^3_N = 8 (1) × 10^{-4} cm^{-1} for the mean nitrogen hyperfine tensor. The principal g values point to a $d(x^2 - y^2)$ electronic ground state, and in conjunction with the hyperfine tensors, they are employed to determine the degree of covalency in the bonding of the Cu(II) impurity to the diamagnetic host lattice and the unpaired electron population in the ligand nitrogens. The EPR results are discussed in terms of the structure of Zn(L-Leu)$_2$ and compared with EPR data in the structurally related Cu(L-Leu)$_2$ complex. Lattice distortions at the impurity sites of Zn(L-Leu)$_2$ are detected and discussed.

Introduction

The crystal and molecular structure and the electronic and magnetic properties of metal–amino acid complexes are subjects of continuous interest for coordination chemists, molecular biologists, and solid-state physicists. These compounds provide in some cases adequate model systems for metalloproteins, and their study is helpful to understand the electronic properties of metal ions in these macromolecules.[2,3] Particularly relevant is the biological role of zinc, which appears to be second to iron among the most important transition-metal ions in living organisms. Most of the zinc-containing proteins that have been identified are enzymes. Biologically, copper is the third most abundant transition-metal element and plays an important role in the active site of some electron-carrying and oxygen-carrying metalloproteins.[4] These characteristics make structural studies of metal–amino acid complexes very useful,[2] particularly for comparison of compounds differing only in the metal ion involved.

Electron paramagnetic resonance (EPR) spectroscopy has played an important role in studying transition-metal-containing proteins and paramagnetic metal–amino acid complexes.[3] In some cases, information about the electronic behavior of metal ions magnetically isolated in diamagnetic metal–amino acid complexes or in pure amino acid hosts is obtained.[5] In other cases the interest resides in the study of the magnetic coupling between neighboring transition-metal ions, particularly the magnitude of the exchange interaction and the possible paths and mechanisms for superexchange between these ions. Related to this case, it has been reported that some copper–amino acid complexes exhibit a quasi-two-dimensional magnetic behavior mediated by exchange interactions of energies much weaker than in other two-dimensional magnetic systems described in the literature.[6]

Besides its magnetic ordering capacity, exchange and superexchange interactions tend to blur most of the fine structure in the EPR spectra. In particular, the differences between the spectra of ions in crystal sites with different ligand field orientations and the features due to hyperfine coupling with the transition-metal nuclei and with the nuclei of the ligands are wiped out. This prevents the obtainment of detailed local information regarding the electronic structure around the paramagnetic ion. To overcome this difficulty, one must use complementary EPR studies on the paramagnetic ion as an impurity in a diamagnetic host lattice structurally isomorphous to the one of interest.

As a part of studies on structural, electronic, and magnetic properties of metal ion–amino acid complexes, we are reporting hereby the synthesis and the crystal and molecular structure of Zn(L-Leu)$_2$. We also report EPR studies on Zn(L-Leu)$_2$ single crystals where low amounts of ^{63}Cu(II) impurities are introduced substitutionally in the position of Zn.

Experimental Section

Sample Preparation. Zn(L-Leu)$_2$ single crystals were obtained by the hydrolysis of urea technique.[7,8] In a typical experiment, a solution of 0.273 g of $ZnCl_2$ (2 mmol), 0.525 g of L-leucine (4 mmol), and 0.120 g of urea (2 mmol) in 200 mL of water was filtered through a Sartorius membrane (0.2 μm pore size), and maintained at 80 °C in a thermostated bath for 1 week. The complex crystallizes as six-faceted transparent plates, which were separated from the hot solution by filtration, washed with water, and air-dried. The largest specimens had approximate dimensions 3 × 1 × 0.3 mm.

Single-crystal samples of copper-substituted Zn(L-Leu)$_2$ for EPR measurements were grown as described above, but now the water solution contained 20 μmol of ^{63}Cu-enriched (98%) copper chloride. Doping with only one isotope improves the EPR resolution that would be achieved by employing naturally occurring copper. This element has two isotopes, ^{63}Cu and ^{65}Cu (natural abundances of 69.09% and 30.91%, respectively), both with nuclear spin $I = {}^3/_2$, whose slightly different nuclear magnetic moments give place to a superposition of two spectra, with a greatly reduced resolution. The Cu/Zn substitution ratio in the samples used for the EPR measurements was estimated to be less than 10^{-3} from the intensity of the EPR signals.

[†] Instituto de Desarrollo Tecnológico para la Industria Química (INTEC).
[‡] Universidad Nacional de La Plata.

(1) (a) Fellow of CONICET. (b) Member of the Carrera del Investigador Cientifico of CONICET, Argentina. (c) Member of the Carrera del Investigador of CICPBA, Argentina.
(2) Freeman, H. C. In *Inorganic Biochemistry*; Eichhorn, G. L., Ed.; Elsevier: Amsterdam, 1973; Chapter 4.
(3) Brill, A. S. *Transition Metal Ions in Biochemistry*; Springer Verlag: Berlin, 1977.
(4) Cotton, F. A.; Wilkinson, G. *Advanced Inorganic Chemistry*; John Wiley and Sons: New York, 1980.
(5) Fujimoto, M.; Janecka, J. *J. Chem. Phys.* **1971**, *55*, 1152. Bonomo, R. P. *J. Chem. Soc., Dalton Trans.* **1983**, 489. Hirasawa, R.; Kon, H. *J. Chem. Phys.* **1972**, *56*, 4467.
(6) Newman, P. R.; Imes, J. L.; Cowen, J. A. *Phys. Rev. B* **1976**, *13*, 4093. Calvo, R.; Mesa, M. A. *Phys. Rev. B* **1983**, *28*, 1244.
(7) Fawcett, T. G.; Ushay, M.; Rose, J. P.; Lalancette, R. A.; Potenza, J. A.; Schugar, H. J. *Inorg. Chem.* **1979**, *15*, 327.
(8) Ou, C. C.; Powers, D. A.; Thich, J. A.; Felthouse, T. R.; Hendrickson, D. N.; Potenza, J. A.; Schugar, H. J. *Inorg. Chem.* **1978**, *17*, 34.

0020-1669/89/1328-1933$01.50/0

Table I. Crystal Data for Zn(L-Leu)$_2$ and Cu(L-Leu)$_2$

	Zn(L-Leu)$_2$	Cu(L-Leu)$_2$[a]
formula	$Zn(C_6H_{12}NO_2)_2$	$Cu(C_6H_{12}NO_2)_2$
mol wt	325.71	323.90
space group	$P2_1$	$P2_1$
a, Å	9.584 (4)	9.725 (4)
b, Å	5.389 (2)	5.127 (1)
c, Å	14.866 (5)	14.689 (6)
β, deg	106.84 (3)	105.79 (3)
V, Å^3	734.9 (9)	704.8 (8)
Z	2	2
ρ_{obsd}, g cm^{-3}	1.47 (2)	1.532 (5)
ρ_{calcd} g cm^{-3}	1.472 (1)	1.525
λ(Mo Kα), Å	0.71069	0.71069
μ, cm^{-1}	16.1	16.3
F_{000}	344	342

[a] Data obtained from ref 7.

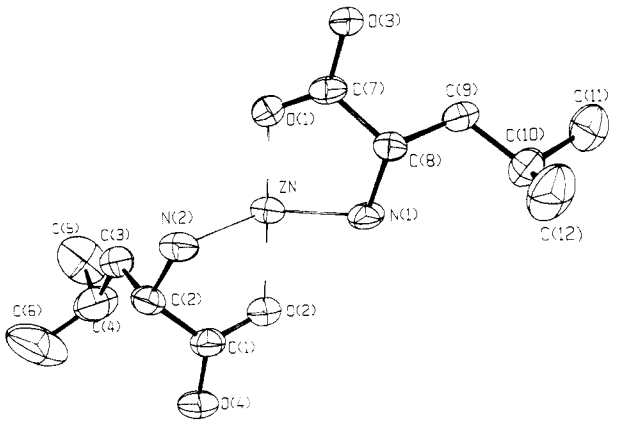

Figure 1. Molecular structure of Zn(L-Leu)$_2$ showing the labeling of atoms and their thermal vibration ellipsoids.

EPR Experiments. The samples are (001) plates with a well-defined $\hat{b}$ axis. They were glued to a cubic shaped sample holder with the $\hat{a}$, $\hat{b}$, and $\hat{c}' = \hat{a} \times \hat{b}$ axes oriented parallel to an xyz reference system defined by the holder ($xyz = abc'$).

The EPR measurements were performed at room temperature in a Bruker ER-200 spectrometer employing Q-band radiation (34 GHz) and a cylindrical cavity with 100-KHz magnetic field modulation. The spectra were taken with the magnetic field applied in three perpendicular planes, xy, zy, and zx, at intervals of 10° along the 180° angular range. The positions in magnetic field strength of the resonances or groups of resonances were measured at each angle. The position of the crystal axes within each plane can be determined with an accuracy of 1°, from the symmetry of the observed gyromagnetic tensors required by the crystal symmetry.

X-ray Diffraction Data. A complete X-ray diffraction data set was obtained at room temperature from a prismatic crystal of approximate dimensions 0.3 × 0.2 × 0.05 mm, with a Huber four-circle diffractometer, used with graphite-monochromated Mo Kα radiation. The unit cell dimensions and matrix orientation for data collection were produced from 16 centered reflections, in the range 4° < θ < 20°, by least-squares refinement. We measured 2898 reflections having θ values in the range 1–25°, by the ω-scan technique working in the step-scan mode. Intensities of three standard reflections were essentially constant throughout the experiment. From 2737 independent reflections in the $\pm h,k,l$ reciprocal space quadrant, 1355 reflections having $I > 3\sigma(I)$ were employed in the calculations. Data were corrected for Lorentz, polarization, extinction, and absorption effects.[9] Transmission factors were in the range 0.718–0.927.

Bonded H atom scattering factors of Stewart et al.,[10] atomic scattering factors of Cromer and Waber,[11] and anomalous dispersion coefficients of Cromer and Ibers[11] for the rest of the atoms were used. Most of the calculations were performed on a PDP 11/34 computer with the SHELX 76 system of programs.[12] The molecular structure and stereoscopic projection were drawn with the program ORTEP.[13]

Crystal Structure Determination and Refinement. The crystal data for Zn(L-Leu)$_2$ are given in Table I, which also includes the data for Cu(L-Leu)$_2$ for comparison purposes.

The position of the zinc ion was already determined from a Patterson map. The rest of the non-hydrogen atoms were located by the usual procedure of alternating cycles of Fourier maps and isotropic least-squares refinement of the molecular fragment determined at each stage. Subsequent anisotropic least-squares refinement converged to an agreement factor $R = \sum||F_o| - |F_c||/\sum|F_o|$ equal to 0.066. At this stage, the hydrogen atoms were included in the model. They were positioned on stereochemical grounds and incorporated with a pair of adjustable isotropic thermal parameters, one for all of the amine H atoms and the other

Table II. Fractional Atomic Coordinates and Equivalent Isotropic Thermal Parameters[16] for Zn(L-Leu)$_2$ with Estimated Standard Deviations in Parentheses

atom	x/a	y/b	z/c	B_{iso}, Å^2
Zn	0.7384 (1)	0.9300 (0)	0.0343 (1)	3.08 (2)
O(1)	0.5487 (6)	1.152 (1)	−0.0003 (4)	3.3 (2)
O(2)	0.9470 (6)	0.768 (2)	0.0606 (4)	3.7 (2)
O(3)	0.3396 (5)	1.200 (1)	−0.1136 (4)	3.6 (2)
O(4)	1.1795 (6)	0.855 (2)	1.1355 (5)	4.9 (2)
N(1)	0.6813 (6)	0.893 (2)	−0.1068 (4)	3.3 (2)
N(2)	0.8659 (7)	1.219 (2)	0.1024 (5)	3.5 (2)
C(1)	1.0461 (7)	0.899 (3)	0.1178 (5)	3.5 (3)
C(2)	0.9974 (8)	1.112 (2)	0.1696 (6)	3.6 (3)
C(3)	0.9545 (9)	1.009 (2)	0.2535 (6)	4.0 (3)
C(4)	1.069 (1)	0.852 (4)	0.3248 (7)	6.8 (6)
C(5)	1.000 (2)	0.721 (4)	0.3935 (9)	7.9 (6)
C(6)	1.194 (1)	1.003 (5)	0.3812 (9)	10.0 (8)
C(7)	0.4728 (8)	1.128 (2)	−0.0813 (6)	2.9 (2)
C(8)	0.4625 (7)	1.512 (2)	0.1545 (6)	3.3 (3)
C(9)	0.4305 (8)	0.833 (2)	−0.2225 (6)	3.8 (3)
C(10)	0.484 (1)	0.738 (2)	−0.3042 (6)	4.3 (3)
C(11)	0.363 (1)	0.582 (3)	−0.3672 (7)	6.0 (4)
C(12)	0.526 (1)	0.939 (4)	−0.3605 (7)	6.8 (4)

Table III. Bond Distances (Å) and Angles (deg) for Zn(L-Leu)$_2$

(a) Bond Distances

Zn–N(2)	2.056 (8)	Zn–N(1)	2.018 (6)
Zn–O(2)	2.112 (6)	Zn–O(1)	2.112 (6)
Zn–O(3')[a]	2.000 (7)	C(7)–O(1)	1.220 (9)
C(1)–O(2)	1.29 (1)	C(7)–O(3)	1.287 (9)
C(1)–O(4)	1.251 (9)	C(7)–C(8)	1.53 (1)
C(1)–C(2)	1.53 (2)	C(8)–N(1)	1.50 (1)
C(2)–N(2)	1.48 (1)	C(9)–C(8)	1.55 (1)
C(3)C(2)	1.53 (1)	C(10)–C(9)	1.54 (1)
C(4)–C(3)	1.54 (2)	C(10)–C(11)	1.52 (2)
C(4)–C(5)	1.54 (2)	C(10)–C(12)	1.49 (2)
C(4)–C(6)	1.49 (2)		

(b) Bond Angles

N(2)–Zn–O(2)	80.0 (3)	C(1)–C(2)–C(3)	109.4 (9)
N(2)–Zn–O(1)	92.2 (3)	C(2)–C(3)–C(4)	117.1 (8)
N(2)–Zn–O(3')	116.7 (3)	C(3)–C(4)–C(5)	110.6 (9)
N(2)–Zn–N(1)	122.0 (4)	C(3)–C(4)–C(6)	113 (1)
O(2)–Zn–O(3')	97.5 (3)	C(5)–C(4)–C(6)	108 (1)
N(1)–Zn–O(1)	81.2 (3)	Zn–O(1)–C(7)	113.9 (6)
N(1)–Zn–O(2)	96.2 (3)	Zn–N(1)–C(8)	112.6 (6)
N(1)–Zn–O(3')	121.1 (3)	O(1)–C(7)–O(3)	125.4 (9)
O(1)–Zn–O(2)	168.9 (3)	O(1)–C(7)–C(8)	119.7 (7)
O(1)–Zn–O(3')	93.0 (3)	O(3)–C(7)–C(8)	114.8 (7)
Zn–O(2)–C(1)	111.9 (7)	C(7)–C(8)–N(1)	110.1 (6)
Zn–N(2)–C(2)	107.8 (6)	C(9)–C(8)–N(1)	112.7 (8)
O(2)–C(1)–O(4)	123 (1)	C(7)–C(8)–C(9)	112.9 (7)
O(2)–C(1)–C(2)	118.1 (7)	C(8)–C(9)–C(10)	114.4 (8)
O(4)–C(1)–C(2)	118.6 (9)	C(9)–C(10)–C(11)	107.6 (9)
C(1)–C(2)–N(2)	106.1 (7)	C(9)–C(10)–C(12)	114 (1)
C(3)–C(2)–N(2)	108.4 (7)	C(11)–C(10)–C(12)	109.8 (8)

[a] The symmetry operation $1 - x$, $y - {}^1/_2$, $-z$ transforms O(3) into O(3').

(9) Busing, W. R.; Levy, H. A. *Acta Crystallogr.* **1957**, *10*, 180.
(10) Stewart, R. F.; Davison, E. R.; Simpson, W. T. *J. Chem. Phys.* **1965**, *42*, 3175.
(11) Cromer, D. T.; Waber, J. T. *International Tables for X-Ray Crystallography*; Kynoch: Birmingham, England, 1974; Vol. IV, p 71. Cromer, D. T.; Ibers, J. A. *Ibid.*, p 149.
(12) Sheldrick, G. M. "SHELX, A Program for Crystal Structure Determination"; University of Cambridge: Cambridge, England, 1976.
(13) Johnson, C. K. "ORTEP"; Report ORNL-3794; Oak Ridge National Laboratory: Oak Ridge, TN, 1965.

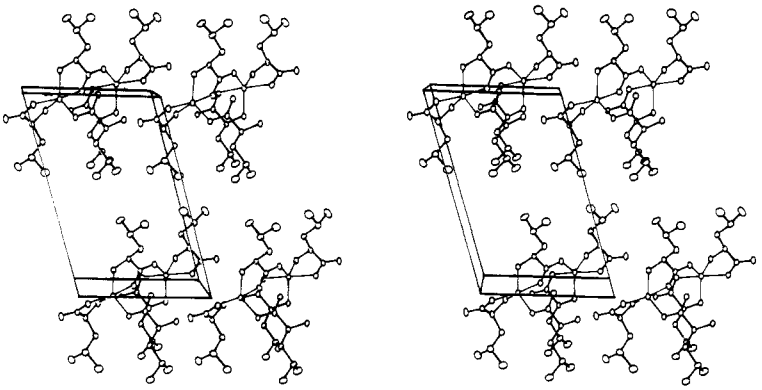

Figure 2. Stereoscopic projection of the crystal packing of $Zn(L\text{-}Leu)_2$ viewed along $\hat{b}$. The $\hat{a}$ axis is horizontal.

for the rest of the hydrogens, into an additional full-matrix least-squares fit where the methyl groups were refined as rigid bodies. In the final cycle, the shifts of the parameters of the non-hydrogen atoms were within 0.001 times their standard deviation.

The final agreement factors R and $R_w = [\sum w(|F_o| - |F_c|)^2/\sum w|F_o|^2]^{1/2}$ were 0.048 and 0.047, respectively, corresponding to a minimization function $M = \sum w(|F_o| - |F_c|)^2$ with weights $w = [\sigma^2(|F_o|) + 0.01|F_c|^2]^{-1}$.

Final positional parameters and equivalent isotropic temperature factors computed by following Hamilton[14] for all non-hydrogen atoms are given in Table II. Figure 1 is a drawing of the molecular structure of $Zn(L\text{-}Leu)_2$ showing the atom-numbering scheme. Figure 2 shows an stereoscopic ORTEP projection of the crystal packing along the $\hat{b}$ axis. Bond distances and angles are given in Table III.

Results and Discussion

Description of the Structure. Comparison with $Cu(L\text{-}Leu)_2$. The crystal and molecular structure of $Zn(L\text{-}Leu)_2$ is closely related to that of $Cu(L\text{-}Leu)_2$ with small but significant differences in the environment around the metal ion. The $Zn(L\text{-}Leu)_2$ complex consists of five-coordinated Zn(II) ions arranged in two-dimensional sheets parallel to the (001) plane. Trans coordination of the two amino acid molecules per zinc ion produces squashed tetrahedral N_2O_2 ligand sets. The average Zn–N and Zn–O bond distances are 2.04 (3) and 2.112 (6) Å, respectively. Additional interaction with one carboxylate oxygen atom from a neighboring ligand [O(3′)] that completes the pentagonal coordination around Zn(II) gives rise to a strong Zn–O bond [d(Zn–O) = 2.000 (7) Å] that forms carboxylate-bridged ZnL_2 units in the sheets (see Figure 2). The ZnL_2 units are further linked within the sheets by weak N–H···O hydrogen bonds.

In comparison, the Cu(II) ion in $Cu(L\text{-}Leu)_2$[7] is tetragonally coordinated at the center of a practically planar (within ±0.05 Å) CuN_2O_2 unit (average Cu–N and Cu–O bond distances of 1.993 (5) and 1.960 (4) Å, respectively). Additional interactions with two carboxylate oxygen atoms from neighboring ligands [O(3′) and O(4′) in ref 7], which complete an elongated octahedral configuration around Cu(II), give rise to weak axial Cu–O bonds (Cu–O bond distances larger than 2.6 Å) that link the CuL_2 units, forming carboxylate-bridged sheets of Cu(II) ions parallel to the ab plane. The CuL_2 units are also linked within the sheets by a net of hydrogen bonds. The Zn–N and Zn–O bond distances in the ZnN_2O_2 units of $Zn(L\text{-}Leu)_2$ are larger than the corresponding equatorial Cu–ligand bond distances in the CuN_2O_2 units of $Cu(L\text{-}Leu)_2$. This can be attributed to the larger ionic radius of Zn(II) (r = 0.76 Å) compared with Cu(II) (r = 0.69 Å).

Calculation of least-squares planes through N_2O_2 ligand sets in $Zn(L\text{-}Leu)_2$ and $Cu(L\text{-}Leu)_2$ complexes (reported as supplementary material) shows that the Zn(II) ion in $Zn(L\text{-}Leu)_2$ is shifted [toward the O(3′) ligand] about 0.6 Å from the mean plane through the distorted tetrahedron N_2O_2; in contrast, the Cu(II) ion in $Cu(L\text{-}Leu)_2$ lies (within ±0.05 Å) on the corresponding equatorial N_2O_2 plane. Both least-squares planes have very similar orientations with respect to the crystal axes. This fact will prove useful later when comparing the EPR spectra of Cu(II) substituted $Zn(L\text{-}Leu)_2$ and of $Cu(L\text{-}Leu)_2$. The torsional angle of 34.0 (3)° between the O(2)O(1)N(2) and O(1)N(2)N(1) planes of $Zn(L\text{-}Leu)_2$ should be compared with the corresponding value of 3.9 (2)° for $Cu(L\text{-}Leu)_2$ and with the perfect tetrahedron value of 70.5°.

In summary, the structures can be related to each other by considering a continuous distortion where the pair of amino acid ligands twist at an angle of about 30°, while the metal ion shifts its position with respect to the mean N_2O_2 molecular plane.

Bond distances and angles for the amino acid ligands (Table III) are in agreement with the corresponding data for the copper complex.[7] They can be compared with previous structural studies on L-leucine hydrobromide[15] and L-leucine hydroiodide,[16] and with the zwitterionic structures of L-leucine[17] and DL-leucine[18] amino acids.

Analysis of the EPR Data. The spin Hamiltonian describing the EPR spectra of the Cu(II) impurities in each crystal site was obtained by considering the crystallographic data for $Zn(L\text{-}Leu)_2$ and assuming that Cu(II) enters substitutionally for Zn(II) in the lattice.[19] We propose the following:

$$H = H_z + H_{Cu} + H_{N1} + H_{N2} \quad (1)$$

with

$$H_z = \mu_B \boldsymbol{S}\cdot\mathbf{g}\cdot\boldsymbol{B} \quad (2a)$$

$$H_{Cu} = \boldsymbol{S}\cdot\mathbf{A}_{Cu}\cdot\boldsymbol{I}_{Cu} \quad (2b)$$

$$H_{N1} = \boldsymbol{S}\cdot\mathbf{A}_{N1}\cdot\boldsymbol{I}_{N1} \quad (2c)$$

$$H_{N2} = \boldsymbol{S}\cdot\mathbf{A}_{N2}\cdot\boldsymbol{I}_{N2} \quad (2d)$$

where μ_B is the Bohr magneton, and $\mathbf{g}$, $\mathbf{A}_{Cu}$, $\mathbf{A}_{N1}$, and $\mathbf{A}_{N2}$ are the gyromagnetic, copper hyperfine, and nitrogen hyperfine tensors, respectively. H_z of eq 2a is the Zeeman interaction of the electronic effective spin $S = {}^1/_2$ of copper with the external magnetic field $\boldsymbol{B}$, which gives rise to one resonance for each copper site. H_{Cu} of eq 2b is the hyperfine interaction with the copper nuclear spin $I_{Cu} = {}^3/_2$ of ^{63}Cu. This interaction splits into four components the resonance for each site. H_{N1} and H_{N2} of eq 2c,d are the hyperfine interactions of $\boldsymbol{S}$ with the nuclear spins $I_{N_\zeta} = 1$ (with ζ = 1, 2) of the two inequivalent ^{14}N ligands. If the nitrogen

(14) Hamilton, W. C. *Acta Crystallogr.* **1959**, *12*, 609.

(15) Subramanian, E. *Acta Crystallogr.* **1967**, *22*, 910.
(16) Chaney, M. O.; Seely, O.; Steinrauf, L. K. *Acta Crystallogr., Sect. B* **1971**, *B37*, 544.
(17) Harding, M. M.; Howieson, R. M. *Acta Crystallogr., Sect. B* **1976**, *B32*, 633. Coll, M.; Solans, X.; Font-Altaba, M.; Subirana, J. A. *Ibid.* **1986**, *C42*, 599.
(18) Di Blasio, B.; Pedone, C.; Sirigu, A. *Acta Crystallogr., Sect. B* **1975**, *B31*, 601.
(19) The actual stereochemistry around Cu(II) in the host lattice may slightly differ from the environment exhibited by Zn(II) ion in $Zn(L\text{-}Leu)_2$ as a result of a modified balance between electronic and steric forces. This effect has been observed in some Cu(II)-substituted Zn(II) host lattices. (a) Hathaway, B. J. *Coord. Chem. Rev.* **1981**, *35*, 211. Hathaway, B.; Duggan, M.; Murphy, A.; Mullane, J.; Power, C.; Walsh, A.; Walsh, B. *Ibid.* **1981**, *36*, 267 and references therein. (b) Reinen, D.; Krause, S. *Inorg. Chem.* **1981**, *20*, 2750. Deeth, R. J.; Hitchman, M. A.; Lehmann, G.; Sachs, H. *Ibid.* **1984**, *23*, 1310.

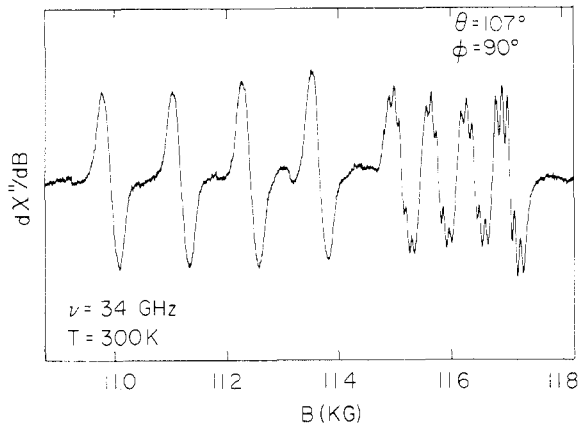

Figure 3. EPR spectrum of ^{63}Cu in a Zn(L-Leu)$_2$ crystal for the magnetic field $\boldsymbol{B}$ oriented in the zy plane at 107° from the $\hat{z}$ axis. Two groups of four lines, corresponding to the two crystallographic sites for copper, are observed. The four-line splitting is due to the $I = {}^3/_2$ nuclear spin of ^{63}Cu. Only the high-field group shows a partially resolved hyperfine structure due to the two nitrogen ligands.

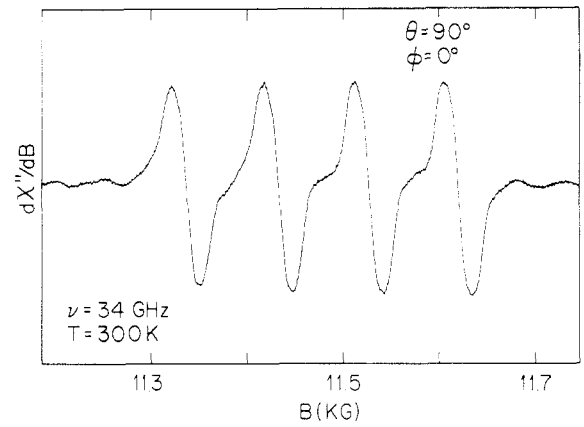

Figure 4. EPR spectrum obtained with $\boldsymbol{B}$ oriented parallel to the $\hat{x}$ axis. The spectra of the two copper sites collapse for this field orientation.

ligands were equivalent through an inversion at the copper position, then $\mathbf{A}_{N1} = \mathbf{A}_{N2}$ and each copper hyperfine resonance would be split into five components with an intensity ratio 1:2:3:2:1. Zn(L-Leu)$_2$ lacks inversion symmetry, and the nitrogens are slightly different. Hence, the ligand hyperfine lines are broadened and the above intensity ratio does not hold exactly.

Our EPR data support the spin Hamiltonian of eq 1 and 2a–d. In the xy and zy planes, we observe two sets of four anisotropic groups of resonances, as shown in Figure 3. These two sets correspond to the two magnetically inequivalent sites for Cu(II) in the crystal. As expected, when the magnetic field is applied along the unique $\hat{b}$ axis or in the zx plane, only one set was observed (see Figure 4). The four groups of each set correspond to the hyperfine coupling with the ^{63}Cu nucleus. For certain orientations of the applied magnetic field the lines show an additional hyperfine structure (see Figure 3) due to the nuclear spins of the two ^{14}N ligands to copper. Since they are not exactly equivalent in Zn(L-Leu)$_2$, these hyperfine structures exhibit broadened lines and hence poor resolution.

Each line of the EPR spectra of one copper site may be labeled by the spin quantum numbers for the copper nucleus (M) and by the nuclei of the nitrogen ligands (m_1, m_2). Then, up to the first order in a perturbative calculation, the position in magnetic field strength of each line (M, m_1, m_2) is given by[20]

$$B(M,m_1,m_2) = \frac{h\nu}{g\mu_B} + \frac{K_{Cu}}{g\mu_B}M + \frac{K_{N1}}{g\mu_B}m_1 + \frac{K_{N2}}{g\mu_B}m_2 + \text{second-order terms} \quad (3)$$

(20) Weil, J. A. *J. Magn. Reson.* **1975**, *18*, 113.

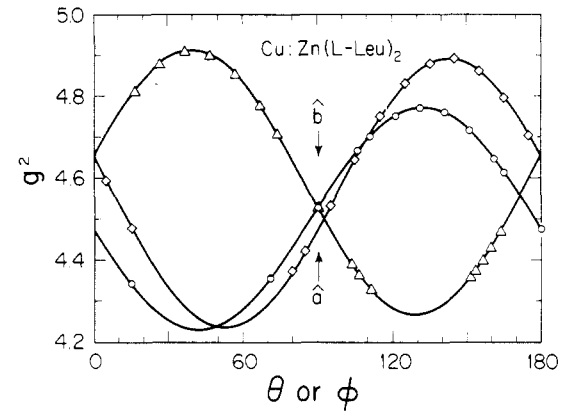

Figure 5. Angular variation of the squared gyromagnetic factor of ^{63}Cu-doped Zn(L-Leu)$_2$, measured at 34 GHz and 300 K, in the xy (○), zy (△), and zx (◇) planes ($xyz \equiv abc'$, $\hat{c}' = \hat{a} \times \hat{b}$). The solid lines are obtained by using the $\mathbf{g}^2$ tensor components tabulated in Table IV.

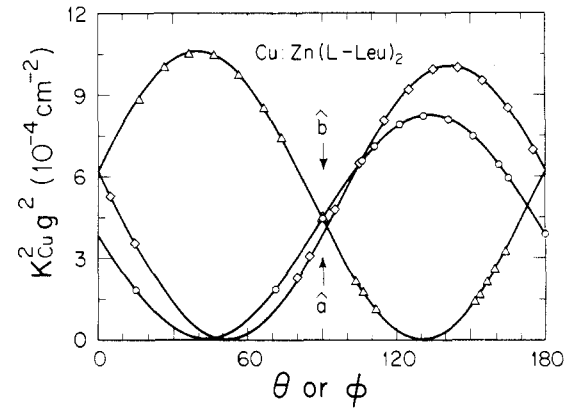

Figure 6. Angular variation of $K^2_{Cu}g^2$ for ^{63}Cu-doped Zn(L-Leu)$_2$, measured in the xy (○), zy (△), and zx (◇) orthogonal planes ($xyz = abc'$, $\hat{c}' = \hat{a} \times \hat{b}$), at 34 GHz. The solid lines are obtained by using the $\mathbf{K}^2_{Cu}\mathbf{g}^2$ tensor given in Table IV.

where h is the Planck constant, ν is the microwave frequency, $M = \pm{}^3/_2, \pm{}^1/_2$, and $m_\zeta = \pm 1, 0$ ($\zeta = 1, 2$). Also

$$g^2 = \hat{h}\cdot\mathbf{g}\cdot\mathbf{g}\cdot\hat{h} \quad (4a)$$

$$K^2_{Cu}g^2 = \hat{h}\cdot\mathbf{g}\cdot\mathbf{A}_{Cu}\cdot\mathbf{A}_{Cu}\cdot\mathbf{g}\cdot\hat{h} \quad (4b)$$

$$K^2_{N_\zeta}g^2 = \hat{h}\cdot\mathbf{g}\cdot\mathbf{A}_{N_\zeta}\cdot\mathbf{A}_{N_\zeta}\cdot\mathbf{g}\cdot\hat{h} \quad (4c)$$

where

$$\hat{h} = \boldsymbol{B}/|\boldsymbol{B}| = \sin\theta\cos\phi, \sin\theta\sin\phi, \cos\theta$$

is a unit vector along $\boldsymbol{B}$. Second-order corrections to the calculated positions of the EPR lines observed at 34 GHz (eq 3) are within experimental error and were not considered.

The values of g^2, $K^2_{Cu}g^2$, and $K^2_{N_\zeta}g^2$ were calculated from the data for each orientation (θ, ϕ) of the applied field $\boldsymbol{B}$ with respect to the $\hat{a}$, $\hat{b}$, and $\hat{c}'$ axes. In the orientation ranges where the hyperfine structure of the ligand nitrogens was not resolved, the observed position of the line was considered as the location of the (M, $m_1 = 0$, $m_2 = 0$) line. From eq 3 and 4a,b, g^2 and $K^2_{Cu}g^2$ were calculated for each orientation of $\boldsymbol{B}$. These experimental values of g^2 and $K^2_{Cu}g^2$, displayed in Figures 5 and 6, were used to determine the components of the $\mathbf{g}^2$ and $\mathbf{K}^2_{Cu}\mathbf{g}^2 = \mathbf{g}\cdot\mathbf{A}_{Cu}\cdot\mathbf{A}_{Cu}\cdot\mathbf{g}$ tensors given in Table IV, by using the least-squares method and eq 4a,b. The calculated parameters are the same in absolute values for the two sites within experimental error. Figures 5 and 6 show the agreement between the experimental values and those obtained from the fitting. Since the copper sites are symmetry related, we show in these figures only the data for one site.

The principal values and directions of the tensors $\mathbf{A}_{Cu}$ and $\mathbf{g}$ were calculated from $\mathbf{g}^2$ and $\mathbf{K}^2_{Cu}\mathbf{g}^2$ and are included in Table V. Similar data were taken for two different samples, and the ei-

Table IV. Values of the Components of the $\mathbf{g}^2$ and $\mathbf{K}^2_{Cu}\mathbf{g}^2$ Tensors for One Site Obtained by a Least-Squares Fit of the g^2 and $K^2_{Cu}g^2$ Data Displayed in Figures 5 and 6[a]

$g^2_{xx} = 4.475$ (1)	$g^2_{xy} = -0.270$ (1)
$g^2_{yy} = 4.527$ (1)	$g^2_{xz} = -0.316$ (1)
$g^2_{zz} = 4.653$ (1)	$g^2_{zy} = 0.317$ (1)
$(K^2_{Cu}g^2)_{xx} = 3.87$ (1)	$(K^2_{Cu}g^2)_{xy} = -4.10$ (1)
$(K^2_{Cu}g^2)_{yy} = 4.44$ (1)	$(K^2_{Cu}g^2)_{xz} = -4.88$ (1)
$(K^2_{Cu}g^2)_{zz} = 6.20$ (1)	$(K^2_{Cu}g^2)_{zy} = 5.23$ (1)

[a] The uncertainties were obtained from the dispersion of the fits. The values corresponding to the other site have the same absolute values within experimental error, but differ in sign in the case of the *xy* and *zy* components. The components of the $\mathbf{K}^2_{Cu}\mathbf{g}^2$ tensor are given in units of 10^{-4} cm^{-2}.

Table V. Eigenvalues and Eigenvectors of the **g** and $\mathbf{A}_{Cu}$ Tensors for One Site[a]

principal values	direction cosines	angles (θ, ϕ), deg
$g^1 = 2.273$ (1)	0.5167, −0.5469, −0.6587	131.2, −46.6
$g^2 = 2.055$ (1)	0.847, 0.441, 0.298	73, 28
$g^3 = 2.066$ (1)	0.127, −0.712, 0.691	46, −80
$A^1_{Cu} = 167.3$ (2)	0.5156, −0.5532, −0.6543	130.9, −47.0
$A^2_{Cu} = 0$ (8)		
$A^3_{Cu} = 11$ (2)		
Cu(L-Leu)$_2$		
$g_\parallel = 2.264$ (2)	0.526, −0.516, 0.677	133, −45
$g_\perp = 2.057$ (2)		

[a] For comparison, we include the values of the molecular *g* factors and the $g_\parallel$ direction, calculated with EPR data at Q-band frequencies in Cu(L-Leu)$_2$ crystals. The eigenvalues of $\mathbf{A}_{Cu}$ are given in units of 10^{-4} cm^{-1}.

genvalues and eigenvectors of **g** and $\mathbf{A}_{Cu}$ obtained from the two sets of data agree within experimental error. The results reported here are those for the sample with the largest signal/noise ratio.

For the field orientation range where the copper hyperfine splitting is the smallest, the copper hyperfine structure is not resolved and we were not able to evaluate g^2 and $K^2_{Cu}g^2$ with any accuracy. This causes a large uncertainty in the values of the tensor $\mathbf{A}_{Cu}$ for those orientations and explains the result $A^2_{Cu} \simeq 0$ obtained for one eigenvalue by extrapolating the result of the fitting performed over experimental points outside of this range.

The hyperfine structure due to the nitrogen ligands is resolved only for ***B*** along a small angular region in the *zy* plane. In this region we were able to observe differences of about 15% between the hyperfine coupling parameters with the two nitrogens. In other angular ranges, the shapes of the resonances are distorted, displaying bumps due to the unresolved ^{14}N hyperfine splitting. This line shape was simulated on a computer to obtain a mean value of the hyperfine coupling with the two nitrogens. In this way, we obtain for the eigenvalues of the mean $\mathbf{A}_N$ tensor the following values:

$$A^1_N = 12\ (1) \times 10^{-4}\ \text{cm}^{-1}$$

$$A^2_N = 9\ (1) \times 10^{-4}\ \text{cm}^{-1}$$

$$A^3_N = 8\ (1) \times 10^{-4}\ \text{cm}^{-1}$$

The eigenvector associated with A^1_N is (0.291, −0.489, 0.822) in the *xyz* crystal axes. The other two eigenvectors could not be obtained due to experimental uncertainties.

The different resolution of the ligand hyperfine structure observed in the four copper hyperfine groups in Figure 3 is due to a dependence of the resonance line widths with M. This arises by a process similar to that described by Froncisz and Hyde.[21] There is a random distribution of molecular orientations around the copper impurities. This leads to a distribution of the **g** and $\mathbf{A}_{Cu}$ tensors whose broadening effects may be appreciated from eq 3.

Allen et al.[22] have reported $g_\parallel = 2.264$ (4), $g_\perp = 2.060$ (8), $A_\parallel = 165$ (4) $\times 10^{-4}$ cm^{-1}, $A_\perp \simeq 30 \times 10^{-4}$ cm^{-1} (for $\mathbf{A}_{Cu}$), and $A_N = 10$ (1) $\times 10^{-4}$ cm^{-1} for polycrystalline samples of Zn(L-Leu)$_2$ doped with copper. These values compare well with ours. Our values, however, being obtained from single-crystal data, are more accurate, and in addition, they provide the principal directions of the gyromagnetic and hyperfine tensors.

Lattice Distortion at the Impurity Site. By comparing the EPR results reported here for Cu:Zn(L-Leu)$_2$ with those obtained in Cu(L-Leu)$_2$ crystals,[23] we may learn about the distortions produced at Zn sites when they are occupied by Cu impurities.

As already commented, the magnetic coupling between neighboring copper ions in Cu(L-Leu)$_2$ blurs the information about local interactions. In this case, one must resort to a model for the determination of the molecular **g** tensor from the measured effective g_{eff} values. These are related to the g_A and g_B values for copper at the crystallographic A and B sites through $g_{eff} = (g_A + g_B)/2$. Assuming axial symmetry around copper, we inferred from EPR data the principal *g* values along the symmetry axis ($g_\parallel$) and perpendicular to it ($g_\perp$) as well as the axis direction for Cu(II) in Cu(L-Leu)$_2$.[23] These data are included in Table V. As expected, the $g_\parallel$ direction is practically coincident with the direction of the normal to the best least-squares plane through the four equatorial ligands of the copper ion.

The **g** and $\mathbf{A}_{Cu}$ diagonal tensors of Cu:Zn(L-Leu)$_2$ have nearly axial symmetry. The principal directions of $g_\parallel = g^1$ and $A_\parallel = A^1_{Cu}$ coincide. A similar comparison between the other two principal directions of **g** and $\mathbf{A}_{Cu}$ is prevented by large uncertainties in the corresponding eigenvectors of $\mathbf{A}_{Cu}$. The values of $g_\parallel$ and $g_\perp$ for Cu(II) in Zn(L-Leu)$_2$ and those measured in Cu(L-Leu)$_2$ crystals are very similar (see Table V). Further, the angle between the orientations for the $g_\parallel$ directions in Zn(L-Leu)$_2$ and Cu(L-Leu)$_2$ is 3°, while the angle between the direction of $g_\parallel$ with the normal to the mean plane through the four ligands in Zn(L-Leu)$_2$ is 10°. Besides that, the eigenvector of A^1_N is along a direction at about 8 and 13° with the directions of the Cu–N(1) and Cu–N(2) bonds in Cu(L-Leu)$_2$ and 40 and 27° with the directions of the Zn–N(1) and Zn–N(2) bonds in Zn(L-Leu)$_2$, respectively. The experimental uncertainty of this direction is about ±4%.

From the above comparisons, we conclude that there are large local distortions at the Zn site in Zn(L-Leu)$_2$ when the Zn is replaced by Cu. Our data indicate that the local environment around Cu impurities in Zn(L-Leu)$_2$ is more similar to that of Cu in Cu(L-Leu)$_2$ than to that of Zn in Zn(L-Leu)$_2$. Local distortion around the metal site in Zn(L-Leu)$_2$ when it is replaced by Cu(II) may be expected due to the appreciable differences between the structures of ligands surrounding the metal sites in Zn(L-Leu)$_2$ and Cu(L-Leu)$_2$ complexes. Our result could be also obtained from electronic spectra with polarized light. However, these data do not exist in Cu-doped Zn(L-Leu)$_2$.

In the case of bis(L-methioninato)zinc(II) doped with Cu(II) impurities, we may expect a much smaller distortion around copper because the local structures at the metal ion site are very much alike in Zn(L-Met)$_2$ and Cu(L-Met)$_2$ complexes.[8,24] The existing EPR data on Cu(II) impurities in Zn(L-Met)$_2$ were taken from powders,[8] and therefore, it is difficult to extract information about local distortions around the copper impurities.

Molecular Orbital Covalence Parameters. Generally, in amino acid complexes, the Cu(II) ions are in an elongated octahedral configuration of negatively charged ligands. This leads to an electronic ground state consisting of a $d(x^2 - y^2)$ copper orbital mixed with ligand orbitals having the same symmetry.[25,26] The

(21) Froncisz, W.; Hyde, I. S. *J. Chem. Phys.* **1980**, *73*, 3123. Hyde, J. S.; Froncisz, W. *Annu. Rev. Biophys. Bioeng.* **1982**, *11*, 391.

(22) Allen, H. C.; Mandrioli, M. I.; Becker, I. W. *J. Chem. Phys.* **1972**, *56*, 997.

(23) Steren, C. A.; Gennaro, A. M.; Levstein, P. R.; Calvo, R. *J. Phys: Condens. Matter* **1989**, *1*, 637.

(24) Wilson, R. B.; de Meester, P.; Hodgson, D. J. *Inorg. Chem.* **1977**, *16*, 1498.

(25) Maki, A. H.; Mc Garvey, B. R. *J. Chem. Phys.* **1958**, *29*, 31.

(26) Kivelson, D.; Neiman, R. *J. Chem. Phys.* **1961**, *35*, 149.

principal values of the **g** and $\mathbf{A}_{Cu}$ tensors can be expressed by[26]

$$g_{\parallel} = g_e - 8\rho(\alpha\beta_1 - U) \quad (5a)$$

$$g_{\perp} = g_e - 2\mu(\alpha\beta - Z) \quad (5b)$$

$$A_{\parallel} = P[\alpha^2(4/7 + K_0) + (g_{\parallel} - g_e) + 3/7(g_{\perp} - g_e) - 8\rho U - 6/7\mu Z] \quad (5c)$$

$$A_{\perp} = P[\alpha^2(2/7 - K_0) + 11/14(g_{\perp} - g_e) - 22\mu Z] \quad (5d)$$

where

$$U = \alpha'\beta_1 S + \alpha'(1 - \beta_1^2)^{1/2}[T(n)]/2$$

$$Z = \alpha'\beta S + \alpha'(1 - \beta^2)^{1/2}[T(n)]/\sqrt{2}$$

$$\rho = \lambda\alpha\beta_1/\Delta E_{xy}$$

$$\mu = \lambda\alpha\beta/\Delta E_{xz,yz}$$

and where $P = g\mu_B g_n \mu_n \langle r^{-3}\rangle_{3d} = 0.036$ cm^{-1}, $g = (g_{\parallel} + 2g_{\perp})/3$, $g_n(^{63}Cu) = 1.4804$ is the nuclear gyromagnetic factor of ^{63}Cu, μ_n is the nuclear magneton, $\lambda = -828$ cm^{-1} is the spin–orbit coupling constant for the free Cu(II) ion, $g_e = 2.0023$ is the free electron value, and $K_0 = 0.43$ is the Fermi contact term for the free Cu(II) ion. Transition energies $\Delta E_{xy} = E_{xy} - E_{x^2-y^2} = 16\,000$ cm^{-1} and $\Delta E_{xz,yz} = E_{xz,yz} - E_{x^2-y^2} = 27\,500$ cm^{-1} were obtained by Allen et al.[22] from optical absorption in powder samples of Cu:Zn(L-Leu)$_2$. We take $T(n) = 0.2765$ as calculated in ref 26. The constants α, α', β, and β_1 are the mixing parameters for the molecular orbitals:

$$\psi B_{1g} = \alpha d_{x^2-y^2} - \alpha'\phi_1(x^2 - y^2)$$

$$\psi A_{1g} = \alpha_1 d_{z^2} - \alpha_1'\phi_1(z^2)$$

$$\psi B_{2g} = \beta_1 d_{xy} - \beta_1'\phi_1(xy)$$

$$\psi E_g = \beta d_{xz} - \beta'\phi_1(xz)$$

$$\psi E_g = \beta d_{yz} - \beta'\phi_1(yz)$$

where the ϕ_1 functions represent the ligand group orbitals of appropriate symmetry. Normalization of the B_{1g} orbital yields

$$\alpha^2 + \alpha'^2 - 2\alpha\alpha' S = 1 \quad (6)$$

where S is the overlap integral.

Following the iterative procedure proposed by Kivelson and Neiman[26] and using our experimental values for $g_{\parallel}$, $g_{\perp} = (g^2 + g^3)/2$ and $A_{\parallel}$, we obtain the following parameters:

$$\alpha^2 = 0.79 \qquad \beta_1^2 = 0.90 \qquad \beta^2 \simeq 1 \qquad K = \alpha^2 K_0 = 0.34$$

The values obtained for α^2 and β_1^2 indicate a covalent character for the in-plane σ and π bonding, respectively, while $\beta^2 \simeq 1$ indicates a ionic out-of-plane π bonding.

Using eq 5e and the calculated covalent parameters, we obtained $A_{\perp} = 24 \times 10^{-4}$ cm^{-1}. This value is roughly on the same order of magnitude as the experimental values and could be taken as an indication of the reliability of the proposed model.

The values of the covalent parameters given above for Cu(II) in Zn(L-Leu)$_2$ are similar to those reported in copper-doped pure amino acid crystals (see ref 5 and 27). They are also similar to those obtained in other copper(II) complexes in which the Cu(II) has an approximately octahedral coordination.[22,26,28]

(27) Misra, B. N.; Kripal, R. C. *Chem. Phys.* **1977**, *19*, 17.

Spin Population in Nitrogen Orbitals. The values of the ^{14}N hyperfine tensor are related to the mixing of s and p orbitals on nitrogens and the unpaired d electron of Cu(II) by the following relations:[29]

$$A^1_N = A_{iso} + 2A_d + 2A_\sigma \quad (7a)$$

$$A^2_N = A^3_N = A_{iso} - A_d - A_\sigma \quad (7b)$$

with

$$A_{iso} = f_s A_s = f_s(8\pi/3)h^{-1}g_n\mu_n g\mu_B|\psi_{2s}(0)|^2 \quad (7c)$$

$$A_\sigma = f_\sigma A_p = f_\sigma(2/5)h^{-1}g_n\mu_n g\mu_B\langle r^{-3}\rangle_{2p} \quad (7d)$$

$$A_d = f_{Cu}g_n\mu_n g\mu_B/R^3 h \quad (7e)$$

In eq 7, f_s and f_σ are the fractions of unpaired electrons in the nitrogen 2s and 2p shells, respectively. $g_n(^{14}N) = 0.40347$ is the nuclear gyromagnetic factor of ^{14}N. $|\psi_{2s}(0)|^2$ is the spin density at the ligand nuclei, and $\langle r^{-3}\rangle_{2p}$ is the expectation value of r^{-3} for a nitrogen 2p electron. R is the Cu–N distance, and f_{Cu} is the fraction of unpaired spin on the copper. The major contribution to the nitrogen tensor is isotropic, and the anisotropic part of the hyperfine interaction tensor has nearly axial symmetry. From eq 7, we evaluate the unpaired electron fractions on the nitrogen orbitals; $f_s = 0.017$, and $f_\sigma = 0.066$. The measured s/p hybridization ratio is $f_s/f_\sigma = 0.258$. This value points to a sp^3 hybridization.

From the normalization condition of the B_{1g} orbital, eq 6, and the calculated unpaired electron fraction on the nitrogen orbitals we obtained $\alpha^2 = 0.76$. This value is in good agreement with that obtained from the **g** and $\mathbf{A}_{Cu}$ tensors.

Summary of the EPR Results. The **g** and $\mathbf{A}_{Cu}$ tensors have nearly axial symmetry. The **g** tensor is similar to that obtained in Cu(L-Leu)$_2$. The axial principal direction is nearer to the normal to the mean ligand plane in Cu(L-Leu)$_2$ than in Zn(L-Leu)$_2$. The direction of A^1_N is closer to the Cu–N bond direction than to the Zn–N direction. The calculated covalence parameters are similar to those in copper-doped amino acids and copper complexes displaying approximate octahedral ligand configuration around Cu(II). The difference between the two nitrogen hyperfine constants indicates, however, that the two Cu–N bonds have different lengths and orientations.

To gather more information about the nitrogen hyperfine coupling and to determine with greater accuracy the environment of copper in the Zn(L-Leu)$_2$ host lattice would require the ENDOR technique.

Acknowledgment. This work was supported by Grants PID 3-905608/85 and 3-907602/85 from the Consejo Nacional de Investigaciones Cientificas y Têcnicas (CONICET), Argentina, and by Grant RG86-14 from the Third World Academy of Sciences (TWAS).

Registry No. Zn(L-Leu)$_2$, 31034-38-5; ^{63}Cu, 14191-84-5; urea, 57-13-6.

Supplementary Material Available: Listings of anisotropic thermal parameters for the non-hydrogen atoms (Table VI), fractional coordinates and isotropic temperature parameters for the hydrogen atoms (Table VII), hydrogen bond distances and angles (Table VIII), and least-squares planes and dihedral and torsional angles for Zn(L-Leu)$_2$ and Cu(L-Leu)$_2$ (Table X) (6 pages); a listing of structure factor amplitudes with standard deviations for Zn(L-Leu)$_2$ (Table IX) (11 pages). Ordering information is given on any current masthead page.

(28) Szabo-Planka, T.; Horvath, L. I. *J. Coord. Chem.* **1984**, *13*, 163.
(29) Zeiger, H. J.; Pratt, G. W. *Magnetic Interactions in Solids*; Clarendon: Oxford, England, 1973.